

NACA RM L53G01

Inactive



RESEARCH MEMORANDUM

LATERAL OSCILLATORY CHARACTERISTICS OF THE
REPUBLIC F-91 AIRPLANE CALCULATED BY USING LOW-SPEED
EXPERIMENTAL STATIC AND ROTARY DERIVATIVES

By Byron M. Jaquet and H. S. Fletcher

Langley Aeronautical Laboratory
Langley Field, Va.

CLASSIFICATION CANCELLED

Authority *NACA R4 3838* Date *7/26/58*

by *M. J. J. 2/16/58* See _____

CLASSIFIED DOCUMENT

This material contains information affecting the National Defense of the United States within the meaning of the espionage laws, Title 18, U.S.C., Secs. 793 and 794, the transmission or revelation of which in any manner to an unauthorized person is prohibited by law.

NATIONAL ADVISORY COMMITTEE FOR AERONAUTICS

WASHINGTON

August 21, 1953

NATIONAL ADVISORY COMMITTEE FOR AERONAUTICS

RESEARCH MEMORANDUM

LATERAL OSCILLATORY CHARACTERISTICS OF THE
REPUBLIC F-91 AIRPLANE CALCULATED BY USING LOW-SPEED
EXPERIMENTAL STATIC AND ROTARY DERIVATIVES

By Byron M. Jaquet and H. S. Fletcher

SUMMARY

The present investigation was conducted to determine, from low-speed tests in the Langley stability tunnel, the static and rotary derivatives of a 1/9-scale model of the Republic F-91 airplane and various of its components (including the effects of wing incidence) and to determine the accuracy with which the period and damping of the lateral oscillation of the airplane could be calculated by using these experimentally determined derivatives (corrected for Mach number effects). Comparisons between flight and calculated period and damping of the lateral oscillation were made for Mach numbers from 0.4 to 0.9 at an altitude of 20,000 feet for 0° wing incidence and several other wing incidences. Some comparisons were made of the static and rotary derivatives of the model and derivatives estimated by available procedures.

The results of the investigation have indicated that the model did not have unusual aerodynamic characteristics except for a large (about -0.125) increment in the damping in yaw contributed by the fuselage. Changes in wing incidence, in general, had little effect on the static and rotary derivatives of the model. The static and rotary derivatives of the model could be estimated with good accuracy only in the low angle-of-attack range by using available procedures.

Changes in the angle between the reference axis and principal axis and in the nondimensional radius of gyration in yaw had only a small effect on the period of the lateral oscillation but had large effects on the damping. This result indicates that, as has been shown in other investigations, knowing the exact mass parameters is as important as knowing the correct derivatives. For the most recent mass characteristics available, good agreement was obtained between the calculated and flight damping for Mach numbers up to 0.6, whereas at higher Mach numbers the calculated rate of damping was greater than that obtained in flight. The calculated period was in good agreement with the flight period for the Mach number range investigated.

INTRODUCTION

An accurate knowledge of the static and rotary stability derivatives and airplane mass characteristics is necessary in order to insure good estimates of the period and damping of the lateral oscillation for any airplane under consideration. Numerous methods are available for the estimation of these derivatives and a number of these methods are summarized in reference 1. In some cases, the derivatives are difficult to estimate, the result being that the period and damping of the lateral oscillation cannot be calculated with the accuracy desired. Such was the case for the Republic F-91 airplane in the investigation reported in reference 2. Generally, poor agreement between calculated and flight values of the period and damping of the lateral oscillation was noted and it was believed that more accurate rolling and yawing derivatives were needed.

The present investigation was conducted to determine from low-speed wind-tunnel tests the static and rotary stability derivatives of a 1/9-scale model of the Republic F-91 airplane and various of its components (including the effects of wing incidence). The static and rotary derivatives of the model components also were estimated by available means for comparison with the experimentally determined derivatives. The experimental derivatives (corrected for Mach number effects) were used to estimate the variation of period and rate of damping of the lateral oscillation with Mach number at an altitude of 20,000 feet for comparison with values obtained from flight tests of the full-scale airplane with 0° wing incidence (ref. 2) and several other wing incidences.

SYMBOLS

The data presented herein are in the form of standard NACA symbols and coefficients of forces and moments and are referred to the stability system of axes shown in figure 1. The center of gravity was at 0.21 of the mean aerodynamic chord. The coefficients and symbols used herein are defined as follows:

C_L	lift coefficient, L/qS_w
C_D	drag coefficient, D/qS_w
C_Y	lateral-force coefficient, Y/qS_w
C_m	pitching-moment coefficient, $M/qS_w\bar{c}_w$
C_l	rolling-moment coefficient, $L'/qS_w b_w$

C_n yawing-moment coefficient, N/qS_wbw

$$C_{L\alpha} = \frac{\partial C_L}{\partial \alpha}$$

$$C_{Y\beta} = \frac{\partial C_Y}{\partial \beta}$$

$$C_{n\beta} = \frac{\partial C_n}{\partial \beta}$$

$$C_{l\beta} = \frac{\partial C_l}{\partial \beta}$$

$$C_{Yp} = \frac{\partial C_Y}{\partial \frac{pb}{2V}}$$

$$C_{np} = \frac{\partial C_n}{\partial \frac{pb}{2V}}$$

$$C_{lp} = \frac{\partial C_l}{\partial \frac{pb}{2V}}$$

$$C_{Yr} = \frac{\partial C_Y}{\partial \frac{rb}{2V}}$$

$$C_{nr} = \frac{\partial C_n}{\partial \frac{rb}{2V}}$$

$$C_{L_r} = \frac{\partial C_L}{\partial \frac{rb}{2V}}$$

L	lift, lb
D	drag, lb
Y	lateral force, lb
M	pitching moment, ft-lb
L'	rolling moment, ft-lb
N	yawing moment, ft-lb
A	aspect ratio, b^2/S
b	span, ft
S	area, sq ft
c	local chord parallel to plane of symmetry, ft
\bar{c}	mean aerodynamic chord, ft, $\frac{2}{b} \int_0^{b/2} c^2 dy$
q	dynamic pressure, lb/sq ft, $\frac{\rho V^2}{2}$
ρ	mass density of air, slugs/cu ft
V	airspeed, ft/sec
y	spanwise distance measured from and perpendicular to plane of symmetry, ft
l	tail length, distance parallel to fuselage reference line from center of gravity to $\bar{c}/4$ of tail, ft
z	tail height, perpendicular distance from fuselage reference line to $\bar{c}/4$ of tail, ft
α	angle of attack of fuselage reference line, deg
n_y	angle-of-attack correction factor to effectiveness of vertical tail in sideslip

β	angle of sideslip, deg or radian (as noted)
i_w	incidence of wing root chord line, deg
$\frac{\partial \sigma_1}{\partial \frac{pb}{2V}}$	rate of change of wing sidewash angle at vertical tail with wing-tip helix angle
$\frac{\partial \sigma_2}{\partial \frac{pb}{2V}}$	rate of change of fuselage sidewash angle at vertical tail with wing-tip helix angle
$pb/2V$	wing-tip helix angle, radian
$rb/2V$	yawing angular velocity parameter, radian
p	rolling velocity, radians/sec
r	yawing angular velocity, radians/sec
ϵ	angle between reference axis and principal axis, positive when reference axis is above principal axis at the nose, deg
η	inclination of principal longitudinal axis with respect to flight path, positive when principal axis is above flight path at nose, deg, $\eta = \alpha - \epsilon$
γ	angle of flight path to horizontal axis, positive in climb, deg
k_{x_0}	radius of gyration in roll about principal longitudinal axis, ft
k_{z_0}	radius of gyration in yaw about principal vertical axis, ft
K_{x_0}	nondimensional radius of gyration in roll about principal longitudinal axis, k_{x_0}/b
K_{z_0}	nondimensional radius of gyration in yaw about principal vertical axis, k_{z_0}/b
$T_{1/2}$	time for oscillation to damp to one-half amplitude, sec
P	period of oscillation, sec
H	altitude, ft

M Mach number
R Reynolds number

Subscripts:

w wing
V vertical tail
H horizontal tail

The following notation is used to denote model components:

F fuselage
W wing
WF wing, fuselage
WVH wing, fuselage, vertical and horizontal tails

The fuselage includes upper and lower rockets and ventral fin unless otherwise noted. (See fig. 2.)

APPARATUS, MODEL, AND TESTS

The Langley 6-foot-diameter rolling-flow test section (ref. 3) and the Langley 6- by 6-foot curved-flow test section (ref. 4) in which rolling or curved flight is simulated by rolling or curving the airstream about a rigidly mounted model were used for the present investigation. The model was mounted on a single support which was rigidly attached to a six-component balance system.

Geometric details of the 1/9-scale model of the Republic F-91 airplane having an inversely tapered, variable-incidence wing are shown in figure 2. Additional details are given in table I. The wing had 40° sweepback of the 0.5 chord line, a taper ratio of 1.63, an aspect ratio of 3.07, an area of 3.95 square feet, a mean aerodynamic chord of 1.178 feet, -5° dihedral, and Republic Aviation Corporation airfoil sections. (See table II.) A center-of-gravity position of 0.21 \bar{c} was selected for the tests and the wing rotation point about which the wing incidence was varied was 0.127 \bar{c} (fig. 2). The model was constructed of laminated mahogany with aluminum inserts in the vertical and horizontal tails and along the wing trailing edge. A photograph of the model is presented as figure 3.

The tests consisted of six-component measurements of forces and moments through an angle-of-attack range of about -8° to 28° . The tests are summarized in the following table:

Test	β , deg	pb/2V	rb/2V	M	R
Static longitudinal	0	0	0	0.17	1.4×10^6
Static lateral	± 5	0	0	.17	1.4
Rolling	0	$\left\{ \begin{array}{l} 0 \\ \pm .0172 \\ \pm .0348 \\ \pm .0522 \end{array} \right\}$	0	.17	1.4
Yawing	0	0	$\left\{ \begin{array}{l} 0 \\ -.0361 \\ -.0765 \\ -.1008 \end{array} \right\}$.13	1.1

The wing, wing-fuselage combination, and the complete model were tested under each of the conditions listed in the table for $i_w = 6^\circ, 0^\circ$, and -2° . The fuselage alone with the top rocket fairing on and off was tested at $\alpha = 0^\circ, 6^\circ, 12^\circ$, and 20° at the values of rb/2V listed in the table.

CORRECTIONS

Approximate jet-boundary corrections derived for unswept wings were applied to the angle of attack and drag coefficient. A correction to C_{Y_r} was applied to account for the pressure gradient associated with curved flow. (See ref. 4.) Blockage corrections, usually less than 1 percent, were not applied to the data nor were support strut tares. Horizontal tail-on pitching moments were corrected for the effects of the jet boundaries by the methods of reference 5.

RESULTS AND DISCUSSION

Wind-Tunnel Data

Basic data.- The basic experimental data obtained during the present investigation are summarized as follows:

Figure

Data:

Variation of C_m , C_D , and C_L with α for $i_w = 6^\circ, 0^\circ, \text{ and } -2^\circ$	4
Variation of C_{Y_β} , C_{n_β} , and C_{l_β} with α for $i_w = 6^\circ, 0^\circ, \text{ and } -2^\circ$	5
Variation of C_{Y_p} , C_{n_p} , and C_{l_p} with α for $i_w = 6^\circ, 0^\circ, \text{ and } -2^\circ$	6
Variation of C_{Y_r} , C_{n_r} , and C_{l_r} with α for $i_w = 6^\circ, 0^\circ, \text{ and } -2^\circ$	7

Some of the basic data are cross-plotted in figure 8 to show the effects of wing incidence on the various derivatives for several lift coefficients.

The basic data do not show unusual static or rolling characteristics when compared to corresponding data for other swept-wing models. (See ref. 6, for example.) The yawing data (fig. 7), however, indicate that the fuselage contributed an unusually large and favorable (negative) increment to C_{n_r} . This increment, about -0.125 , is as large as that contributed by the vertical tail of other models (see, for example, ref. 7).

Effects of wing incidence.- The effects of wing incidence on the static longitudinal stability characteristics can be seen from the basic data of figure 4. The primary effect of wing incidence is to change the angle of zero lift by an amount approximately equal to the change in incidence.

The effects of wing incidence on the static lateral and rotary stability derivatives are shown in figure 8, for several lift coefficients, for the complete model, wing-fuselage combination, and the tail contribution. The tail contribution to the various derivatives was determined by subtracting the wing-fuselage derivatives from the complete model derivatives. Wing incidence, in general, has only a small

effect on the wing-fuselage-combination derivatives. The tail contribution to some of the derivatives is affected somewhat by a change in wing incidence, and this effect is probably caused by a displacement of the wing wake relative to the vertical tail as the wing incidence is changed. (See ref. 8 for the effects of the wing wake on the rolling derivatives of vertical tails.)

Comparison of Measured and Estimated Derivatives

Vertical-tail contributions.— The equations, and their source, used to calculate the vertical-tail increments of the various derivatives are as follows:

Equations	Reference
$(C_{Y\beta})_V = -(C_{L\alpha})_V \frac{S_V}{S_W} n_Y$	9
$(C_{n\beta})_V = -(C_{Y\beta})_V \left(\frac{l_V}{b_W} \cos \alpha + \frac{z_V}{b_W} \sin \alpha \right)$	10
$(C_{l\beta})_V = -(C_{Y\beta})_V \left(\frac{l_V}{b_W} \sin \alpha - \frac{z_V}{b_W} \cos \alpha \right)$	10
$(C_{Yp})_V = -(C_{L\alpha})_V \frac{S_V}{S_W} \left[\frac{2}{b_W} (z_V \cos \alpha - l_V \sin \alpha) - \left(\frac{\partial \sigma_1}{\partial \beta b} + \frac{\partial \sigma_2}{\partial \beta b} \right) \right]$	11
$(C_{np})_V = (C_{L\alpha})_V \frac{S_V}{S_W} \frac{1}{b_W} (z_V \sin \alpha + l_V \cos \alpha) \left[\frac{2}{b_W} (z_V \cos \alpha - l_V \sin \alpha) - \left(\frac{\partial \sigma_1}{\partial \beta b} + \frac{\partial \sigma_2}{\partial \beta b} \right) \right]$	11
$C_{l_{pV}} = -(C_{L\alpha})_V \frac{S_V}{S_W} \frac{1}{b_W} (z_V \cos \alpha - l_V \sin \alpha) \left[\frac{2}{b_W} (z_V \cos \alpha - l_V \sin \alpha) - \left(\frac{\partial \sigma_1}{\partial \beta b} + \frac{\partial \sigma_2}{\partial \beta b} \right) \right]$	11
$(C_{Yr})_V = 2(C_{L\alpha})_V \frac{S_V}{S_W} \left(\frac{l_V}{b_W} \cos \alpha + \frac{z_V}{b_W} \sin \alpha \right)$	7
$(C_{nr})_V = -2(C_{L\alpha})_V \frac{S_V}{S_W} \left(\frac{l_V}{b_W} \cos \alpha + \frac{z_V}{b_W} \sin \alpha \right)^2$	7
$(C_{lr})_V = 2(C_{L\alpha})_V \frac{S_V}{S_W} \left(\frac{l_V}{b_W} \cos \alpha + \frac{z_V}{b_W} \sin \alpha \right) \left(\frac{z_V}{b_W} \cos \alpha - \frac{l_V}{b_W} \sin \alpha \right)$	7

The quantity $(C_{L\alpha})_V$ is per radian.

The lift-curve slope $(C_{L\alpha})_v$ was determined from reference 12 for an effective aspect ratio determined from reference 9. When the yawing and rolling derivatives of the vertical tail were calculated, the effective aspect ratio was considered to be equal to the geometric aspect ratio with no end-plate effect of the fuselage. (See ref. 7 for the yawing case.) The factors $\frac{\partial \sigma_1}{\partial \frac{pb}{2V}}$ and $\frac{\partial \sigma_2}{\partial \frac{pb}{2V}}$ were obtained from references 8 and 11, respectively.

The rolling and yawing derivatives of the vertical tail were also calculated by using the experimental static derivatives.

The horizontal-tail contribution to C_{L_p} was calculated by the method given in reference 13.

The estimated tail contributions to the various derivatives are compared with the experimental values in figure 9. In general, the tail contributions to the rotary derivatives could be estimated with fairly good accuracy by using the estimated $(C_{L\alpha})_v$ but, when the experimental static derivatives were used, the agreement was poorer especially at moderate and high angles of attack. This result has been previously noted for the yawing case in the investigation reported in reference 7.

The poorer agreement obtained when experimental static-lateral stability derivatives are used to calculate rotary derivatives of the tail is the result of different types of flow. In sideslip, the flow direction along the length of the fuselage is constant; whereas, in the yawing case, the flow direction varies along the fuselage length and, consequently, the influence of the fuselage in sideslip and yawing flow is considerably different (ref. 7). The effects of the fuselage on the sidewash at the tail for the rolling case are discussed in reference 11.

Wing-fuselage contribution.- The wing-fuselage-combination derivatives were taken as the sum of the wing derivatives and fuselage derivatives. Estimated values of the wing and fuselage derivatives were obtained from the following sources:

Component	Derivative	Reference
Wing	C_{l_β} , C_{n_β} , C_{Y_β} , C_{l_r} , C_{n_r} , C_{Y_r}	14
Wing	C_{l_p}	15
Wing	C_{Y_p} , C_{n_p}	16
Fuselage	C_{Y_β} , C_{n_β}	9
Fuselage	C_{Y_r} , C_{n_r}	7
Fuselage	C_{Y_p} , C_{n_p}	10
Fuselage	C_{l_β} , C_{l_r} , $C_{l_p}^1$	--

¹These values are assumed to be zero.

The effect of wing dihedral on C_{Y_p} was determined from reference 17 and on C_{l_β} and C_{l_r} from reference 18. The contribution of the rocket fairings to C_{Y_r} and C_{n_r} was determined by assuming the fairings to be low-aspect-ratio vertical fins. These contributions were calculated by using the equations for $(C_{n_r})_V$ and $(C_{Y_r})_V$ as given in a previous section.

The measured and estimated wing-fuselage-combination derivatives are compared in figure 10. In general, the agreement is good at low angles of attack but is poor at high angles of attack. The large differences between estimated and experimental values of C_{l_β} , C_{l_r} , and C_{Y_p} may be attributed to the fact that the theory of references 14 and 16 does not account for the flow separation that occurs at angles of attack appreciably below the stall at low Reynolds numbers. It is believed that these estimated curves may indicate trends at higher Reynolds numbers. The differences for the other derivatives may be attributable to mutual interference effects of the wing-fuselage combination which have not been accounted for since interference effects have been determined only for simple bodies of revolution. (See refs. 7, 9, and 11.) In addition, the canopy may have some effect on the various derivatives. (See ref. 19.)

Complete model.— The complete-model derivatives were obtained by the addition of the wing-fuselage and vertical-tail derivatives. A

comparison of the estimated and experimental derivatives (fig. 11) indicates generally good agreement at low angles of attack but poor agreement at angles of attack above about 8° . The poor agreement at high angles of attack is a direct consequence of the poor agreement of the estimated and experimental wing-fuselage derivatives.

Estimated Effects of Mach Number on Derivatives

Inasmuch as the derivatives shown in figures 4 to 7 were obtained at Mach numbers near zero in order to make them applicable for calculating the airplane stability at Mach numbers up to 0.9, it was necessary to apply corrections for Mach number effects. This was accomplished by correcting the vertical-tail derivatives and wing-fuselage derivatives independently. Aeroelastic or unsteady lift effects on the derivatives have been neglected.

Vertical tail.- The lift-curve slope of the vertical tail was obtained from the experimental derivative $(C_{Y_\beta})_V$ and, for this lift-curve slope, an effective aspect ratio was determined from reference 12. From reference 20 the effects of Mach number on the vertical-tail lift-curve slope were determined and these corrections were applied to all vertical-tail derivatives.

Wing-fuselage combination.- The lift-curve slope of the airplane for Mach numbers from 0.6 to 0.9 was obtained from reference 21. Lift-curve slopes for Mach numbers between those of the present investigation and those of reference 21 were obtained by fairing a curve between the values of C_{L_α} at $M = 0.17$ and $M = 0.60$. Reference 20 was used to obtain Mach number corrections for C_{l_β} , C_{l_r} , C_{l_p} , C_{n_p} , and C_{Y_p} . The wing-fuselage contributions to the derivatives C_{Y_β} , C_{n_β} , C_{n_r} , and C_{Y_r} were assumed to be constant for the Mach number range considered since the fuselage is generally the primary contributor to these derivatives and Mach number corrections for fuselages are generally considered negligible in the subsonic speed range.

Complete model.- The complete-model derivatives are the sum of the corrected vertical-tail derivatives and the corrected wing-fuselage derivatives for a given angle of attack and Mach number. The variation of C_L and the static and rotary derivatives with Mach number for several angles of attack are presented in figure 12 for wing incidences of 6° , 0° , and -2° .

Lateral Oscillatory Characteristics

Several values of the mass parameters $K_{Z_0}^2$ and ϵ were available for the Republic F-91 airplane from the Ames Aeronautical Laboratory. Because there was no indication of which values were correct, the period and damping (presented in terms of the time to damp to half amplitude) of the lateral oscillation were calculated by using the range of values of $K_{Z_0}^2$ and ϵ shown in table III and the aerodynamic derivatives of figure 12. The calculations were made for an altitude of 20,000 feet, a wing loading of 61.1 pounds per square foot, and a relative density factor of 47.9 by using the linearized equations of lateral motion as presented in reference 22. All calculations were made on an automatic digital computing machine.

Effects of ϵ and $K_{Z_0}^2$ on calculated period and damping.- A decrease in ϵ from 6° to 0° for the two larger values of $K_{Z_0}^2$ (figs. 13(a) and 13(b)) results in a decrease in $T_{1/2}$ (indicating an increase in damping) and P with ϵ having a large effect on the damping at low Mach numbers and a small effect at $M = 0.9$. For the smallest value of $K_{Z_0}^2$ (fig. 13(c)), ϵ has a negligible effect on the damping and period except at low Mach numbers. Decreasing $K_{Z_0}^2$ for a constant value of ϵ decreases both $T_{1/2}$ and P with the largest effect at low Mach numbers.

Comparison of flight and calculated period and damping.- The dashed curves in figure 13 represent flight data which were obtained from reference 2. The flight $T_{1/2}$ has a smaller variation with Mach number than the calculated values. The best agreement between calculated and flight values of the damping is obtained when $K_{Z_0}^2 = 0.1026$ and $\epsilon = 0^\circ$ (fig. 13(a)) for Mach numbers up to 0.6 and for higher Mach numbers the calculated curve indicates greater damping than actually exists. The corresponding calculated period is about 10 percent lower than the flight values for the Mach number range investigated.

A comparison of the effect of using estimated derivatives or experimental derivatives in the calculation of the variation of the damping and period with Mach number is presented in figure 14 for two different sets of mass data; the mass data used for the calculations of figure 14(b) are the most recent available for the airplane (ref. 2).

For the mass data used in figure 14(a) there is little difference in the damping and period when either estimated or experimental derivatives are used in the calculations. When estimated or experimental derivatives are used with the most recent mass data (fig. 14(b)), a

large difference in the calculated damping results; the calculated trend of damping with Mach number using experimental derivatives approaches the flight trend, whereas the calculations using estimated derivatives indicate less damping at low Mach numbers and a greater change in damping with an increase in Mach number. Calculations were also made (data not presented) for the conditions of figure 14(a) with experimental derivatives neglecting Mach number corrections. These calculations resulted in values of $T_{1/2}$ and P that were almost identical to the values in figure 14(a). This is probably the results of compensating effects of the Mach number corrections (theoretical) and, if experimental Mach number corrections had been available, this may not have happened.

Large differences in some of the derivatives of reference 2 (estimated) and the present paper (experimental derivatives) are apparent, notably $C_{Y\beta}$, $C_{l\beta}$, C_{l_r} , and C_{n_r} . As was noted previously, the differences obtained in calculating $T_{1/2}$ and P by using estimated and experimental derivatives may or may not be large depending on the mass parameters and these differences in derivatives are incidental in some cases and are important in others. This result indicates that knowing the exact mass parameters of an airplane is as important as knowing the correct derivatives.

There are other items that could possibly affect the calculations. One of these is random control movement. In the investigation of reference 2 it was noted that the controls were assumed fixed although this was not known to be a certainty. On the basis of the investigation of reference 23, random control movement could have an appreciable effect on the motions of the airplane and it was necessary to account for this in the calculations. Time histories for the subject airplane were not available and, hence, the effects of control movement have not been included in the calculations.

It is also possible that the Mach number effects on the derivatives are not predictable by the currently available theoretical methods for Mach numbers above 0.75 and this may have an effect on the variation of the damping with Mach number.

Effects of wing incidence on period and damping. - For the calculations to determine the effects of wing incidence on the period and damping of the lateral oscillation it was assumed that wing incidence did not affect $K_{x_0}^2$, $K_{z_0}^2$, and ϵ . The value of $K_{z_0}^2$ was 0.1026 for all calculations, and values of ϵ of 0° and 3° were used as is noted in table III.

The effects of wing incidence on the variation of $T_{1/2}$ and P with Mach number are shown in figure 15(a) and these data are cross-plotted in figure 15(b) to show the variation of $T_{1/2}$ and P with wing incidence for the Mach number range investigated. Also shown in figure 15(b) are flight values of $T_{1/2}$ and P for several wing incidences as obtained from the NACA High Speed Flight Research Station at Edwards Air Force Base, Calif. (to date unpublished). For either value of ϵ , decreasing the wing incidence from 6° to -2° decreases the time to damp to one-half amplitude, the effect of incidence decreasing as the Mach number is increased. Except for a Mach number of 0.5, $T_{1/2}$ decreases linearly with a decrease in wing incidence for either value of ϵ . Wing incidence has little effect on the period of the oscillation, the period for $i_w = 0^\circ$ being slightly higher than for other values of i_w . These trends are generally similar to those obtained in the flight tests, although for incidences greater than 4° the flight data indicate a greater decrease in damping with an increase in wing incidence than was calculated. The magnitude of $T_{1/2}$ varies with ϵ for a given Mach number and, for $\epsilon = 0^\circ$, the calculated magnitude of $T_{1/2}$ is about the same as that obtained in flight for Mach numbers up to 0.6.

CONCLUSIONS

An investigation was conducted to determine, from low-speed tests in the Langley stability tunnel, the static and rotary derivatives of a 1/9-scale model of the Republic F-91 airplane and to determine the accuracy with which the period and damping of the lateral oscillation of the airplane could be calculated by using these experimentally determined derivatives (corrected for Mach number effects). Comparisons were made between flight and calculated period and damping of the lateral oscillation for Mach numbers from 0.4 to 0.9 at an altitude of 20,000 feet for 0° wing incidence and several other wing incidences. Some comparisons were made of the static and rotary derivatives of the model and derivatives estimated by available procedures. The results of the investigation indicate the following conclusions:

1. The model did not have unusual aerodynamic characteristics except for a large (-0.125) increment in the damping in yaw contributed by the fuselage.

2. Changes in wing incidence, in general, had little effect on the static and rotary derivatives of the model.

3. The static and rotary stability derivatives of the model could be estimated with good accuracy only in the low angle-of-attack range by using available procedures.

4. Changes in the angle between the principal axis and the reference axis and in the nondimensional radius of gyration in yaw had only a small effect on the period of the oscillation but had large effects on the damping. This result indicates that, as has been shown in other investigations, knowing the exact mass parameters is as important as knowing the correct derivatives.

5. For the most recent mass characteristics available, good agreement was obtained between the calculated and flight damping for Mach numbers up to 0.6, whereas, at higher Mach numbers, the calculated rate of damping was greater than that obtained in flight. The calculated period was in good agreement with the flight period for the Mach number range investigated.

Langley Aeronautical Laboratory,
National Advisory Committee for Aeronautics,
Langley Field, Va., June 24, 1953.

REFERENCES

1. Campbell, John P., and McKinney, Marion O.: Summary of Methods for Calculating Dynamic Lateral Stability and Response and for Estimating Lateral Stability Derivatives. NACA Rep. 1098, 1952. (Supersedes NACA TN 2409.)
2. Heinle, Donovan R., and McNeill, Walter E.: Correlation of Predicted and Experimental Lateral Oscillation Characteristics for Several Airplanes. NACA RM A52J06, 1952.
3. MacLachlan, Robert, and Letko, William: Correlation of Two Experimental Methods of Determining the Rolling Characteristics of Unswept Wings. NACA TN 1309, 1947.
4. Bird, John D., Jaquet, Byron M., and Cowan, John W.: Effect of Fuselage and Tail Surfaces on Low-Speed Yawing Characteristics of a Swept-Wing Model As Determined in Curved-Flow Tests Section of the Langley Stability Tunnel. NACA TN 2483, 1951. (Supersedes NACA RM L8G13.)
5. Gillis, Clarence L., Polhamus, Edward C., and Gray, Joseph L., Jr.: Charts for Determining Jet-Boundary Corrections for Complete Models in 7- by 10-Foot Closed Rectangular Wind Tunnels. NACA WRL-123, 1945. (Formerly NACA ARR L5G31.)
6. Bird, John D., Lichtenstein, Jacob H., and Jaquet, Byron M.: Investigation of the Influence of Fuselage and Tail Surfaces on Low-Speed Static Stability and Rolling Characteristics of a Swept-Wing Model. NACA TN 2741, 1952. (Supersedes NACA RM L7H15.)
7. Letko, William: Effect of Vertical-Tail Area and Length on the Yawing Stability Characteristics of a Model Having a 45° Sweptback Wing. NACA TN 2358, 1951.
8. Michael, William H., Jr.: Analysis of the Effects of Wing Interference on the Tail Contributions to the Rolling Derivatives. NACA Rep. 1086, 1953. (Supersedes NACA TN 2332.)
9. Queijo, M. J., and Wolhart, Walter D.: Experimental Investigation of the Effect of Vertical-Tail Size and Length and of Fuselage Shape and Length on the Static Lateral Stability Characteristics of a Model With 45° Sweptback Wing and Tail Surfaces. NACA Rep. 1049, 1951. (Supersedes NACA TN 2168.)

10. Letko, William, and Riley, Donald R.: Effect of an Unswept Wing on the Contribution of Unswept-Tail Configurations to the Low-Speed Static- and Rolling-Stability Derivatives of a Midwing Airplane Model. NACA TN 2175, 1950.
11. Wolhart, Walter D.: Influence of Wing and Fuselage on the Vertical-Tail Contribution to the Low-Speed Rolling Derivatives of Midwing Airplane Models With 45° Sweptback Surfaces. NACA TN 2587, 1951.
12. DeYoung, John: Theoretical Additional Span Loading Characteristics of Wings With Arbitrary Sweep, Aspect Ratio, and Taper Ratio. NACA TN 1491, 1947.
13. McNeill, Walter E., and Cooper, George E.: A Comparison of Measured and Predicted Lateral Oscillatory Characteristics of a 35° Swept-Wing Fighter Airplane. NACA RM A51C28, 1951.
14. Toll, Thomas A., and Queijo, M. J.: Approximate Relations and Charts for Low-Speed Stability Derivatives of Swept Wings. NACA TN 1581, 1948.
15. Goodman, Alex, and Adair, Glenn H.: Estimation of the Damping in Roll of Wings Through the Normal Flight Range of Lift Coefficient. NACA TN 1924, 1949.
16. Goodman, Alex, and Fisher, Lewis R.: Investigation at Low-Speeds of the Effect of Aspect Ratio and Sweep on the Rolling Stability Derivatives of Untapered Wings. NACA Rep. 968, 1950. (Supersedes NACA TN 1835.)
17. Queijo, M. J., and Jaquet, Byron M.: Calculated Effects of Geometric Dihedral on the Low-Speed Rolling Derivatives of Swept Wings. NACA TN 1732, 1948.
18. Queijo, M. J., and Jaquet, Byron M.: Investigation of Effects of Geometric Dihedral on Low-Speed Static Stability and Yawing Characteristics of an Untapered 45° Sweptback-Wing Model of Aspect Ratio 2.61. NACA TN 1668, 1948.
19. Fisher, Lewis R., and Michael, William H., Jr.: An Investigation of the Effect of Vertical-Fin Location and Area on Low-Speed Lateral Stability Derivatives of a Semitailless Airplane Model. NACA RM L51A10, 1951.
20. Fisher, Lewis R.: Approximate Corrections for the Effects of Compressibility on the Subsonic Stability Derivatives of Swept Wings. NACA TN 1854, 1949.

21. Mitcham, Grady L., and Blanchard, Willard S., Jr.: Summary of the Aerodynamic Characteristics and Flying Qualities Obtained From Flights of Rocket-Propelled Models of an Airplane Configuration Incorporating a Sweptback Inversely Tapered Wing at Transonic and Low-Supersonic Speeds. NACA RM L50G18a, 1950.
22. Sternfield, Leonard: Effect of Automatic Stabilization on the Lateral Oscillatory Stability of a Hypothetical Airplane at Supersonic Speeds. NACA TN 1818, 1949.
23. Bird, John D., and Jaquet, Byron M.: A Study of the Use of Experimental Stability Derivatives in the Calculation of the Lateral Disturbed Motions of a Swept-Wing Airplane and Comparison With Flight Results. NACA Rep. 1031, 1951. (Supersedes NACA TN 2013.)

TABLE I.- GEOMETRIC CHARACTERISTICS OF 1/9-SCALE MODEL
OF REPUBLIC F-91 AIRPLANE

Wing:

Aspect ratio	3.07
Taper ratio	1.63
Quarter-chord sweep angle, deg	37.5
Dihedral angle, deg	-5
Incidence, variable, deg	-2 to 6
Area, sq ft	3.95
Span, ft	3.485
Mean aerodynamic chord, ft	1.178
Tip chord, ft	1.43

Vertical tail:

Aspect ratio	2.18
Taper ratio	0.39
Quarter-chord sweep angle, deg	33
Area from fuselage reference line, sq ft	0.768
Span from fuselage reference line, ft	1.293
Mean aerodynamic chord, ft	0.632
Tail-length ratio, l_V/b_W	0.499
Tail-height ratio, z_V/b_W	0.159
Area ratio, S_V/S_W	0.195
Tip chord, ft	0.333

Horizontal tail:

Aspect ratio	3.90
Taper ratio	1.0
Quarter-chord sweep angle, deg	40
Dihedral angle, deg	0
Incidence, deg	0
Area ratio, S_H/S_W	0.223
Span, ft	1.852
Tail-length ratio, l_H/\bar{c}_W	1.785
Tail-height ratio, z_H/\bar{c}_W	0.425

Fuselage:

Length, ft	4.81
Maximum depth excluding canopy, ft	0.676

TABLE II.- WING AIRFOIL COORDINATES PARALLEL TO PLANE OF SYMMETRY

[Obtained from ref. 21]

Station, percent chord	Root section		Tip section	
	Upper, percent chord	Lower, percent chord	Upper, percent chord	Lower, percent chord
0.0	0	0	0	0
.5	.63	.51	.66	.54
.75	.78	.64	.81	.67
1.25	1.01	.82	1.05	.86
2.50	1.44	1.15	1.48	1.19
5.00	2.05	1.60	2.09	1.63
7.50	2.52	1.92	2.53	1.94
10.00	2.88	2.17	2.89	2.18
15	3.44	2.53	3.44	2.53
20	3.84	2.78	3.84	2.78
25	4.13	2.94	4.13	2.94
30	4.32	3.04	4.32	3.04
35	4.44	3.08	4.44	3.08
40	4.48	3.08	4.48	3.08
45	4.45	3.01	4.45	3.01
50	4.36	2.89	4.36	2.89
55	4.15	2.72	4.15	2.72
60	3.89	2.50	3.89	2.50
65	3.57	2.23	3.57	2.23
70	3.19	1.93	3.19	1.93
75	2.75	1.60	2.75	1.60
80	2.27	1.25	2.27	1.25
85	1.75	.89	1.75	.89
90	1.21	.54	1.21	.54
95	.63	.24	.63	.24
100	0	0	0	0

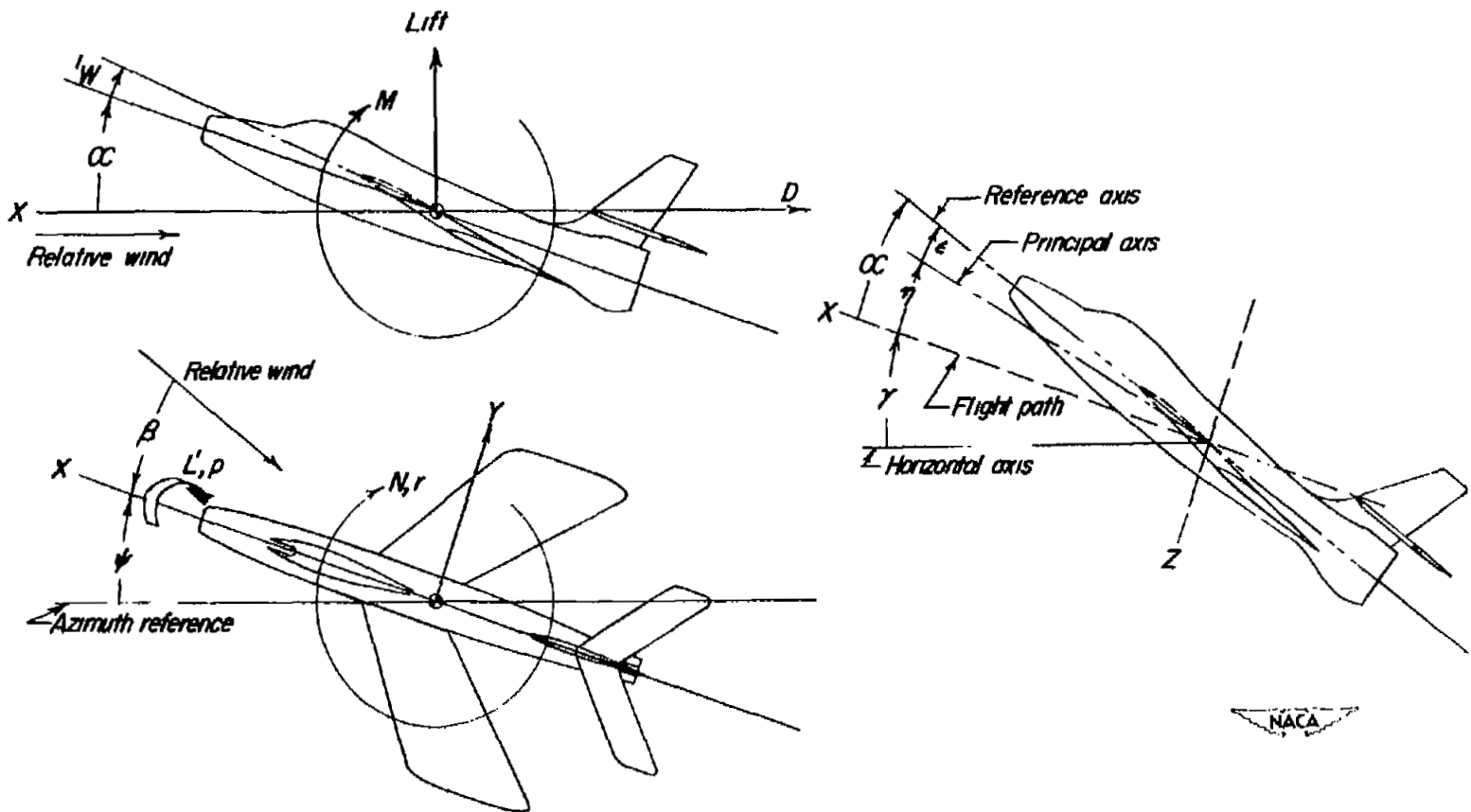
TABLE III.- FLIGHT CONDITIONS

[Investigated at an altitude of 20,000 ft, a wing loading of 61.1 lb/sq ft, and $i_w = 0^\circ$]

Mach number	C_L	$K_{X_0}^2$	$K_{Z_0}^2$	ϵ , deg
			(a)	(a)
0.4	0.560	0.02455	0.1026	6, 3, 0
		.02455	.0941	6, 3, 0
		.02455	.0544	6, 3, 0
		.0249	.0887	1.5
.5	.357	.02455	.1026	6, 3, 0
		.02455	.0941	6, 3, 0
		.02455	.0544	6, 3, 0
		.0249	.0887	1.5
.6	.248	.02455	.1026	6, 3, 0
		.02455	.0941	6, 3, 0
		.02455	.0544	6, 3, 0
		.0249	.0887	1.5
.7	.183	.02455	.1026	6, 3, 0
		.02455	.0941	6, 3, 0
		.02455	.0544	6, 3, 0
		.0249	.0887	1.5
.8	.140	.02455	.1026	6, 3, 0
		.02455	.0941	6, 3, 0
		.02455	.0544	6, 3, 0
		.0249	.0887	1.5
.9	.110	.02455	.1026	6, 3, 0
		.02455	.0941	6, 3, 0
		.02455	.0544	6, 3, 0
		.0249	.0887	1.5

^aFor $i_w = 6^\circ$ and -2° , values of ϵ used were 0° and 3° , $K_{Z_0}^2$ was 0.1026, and $K_{X_0}^2$ was 0.02455.





(a) Stability system of axes. Arrows indicate positive direction of forces, moments, and angular velocities.

(b) System of axes and angular relationship in flight. Arrows indicate positive direction of angles.

Figure 1.- System of axes.

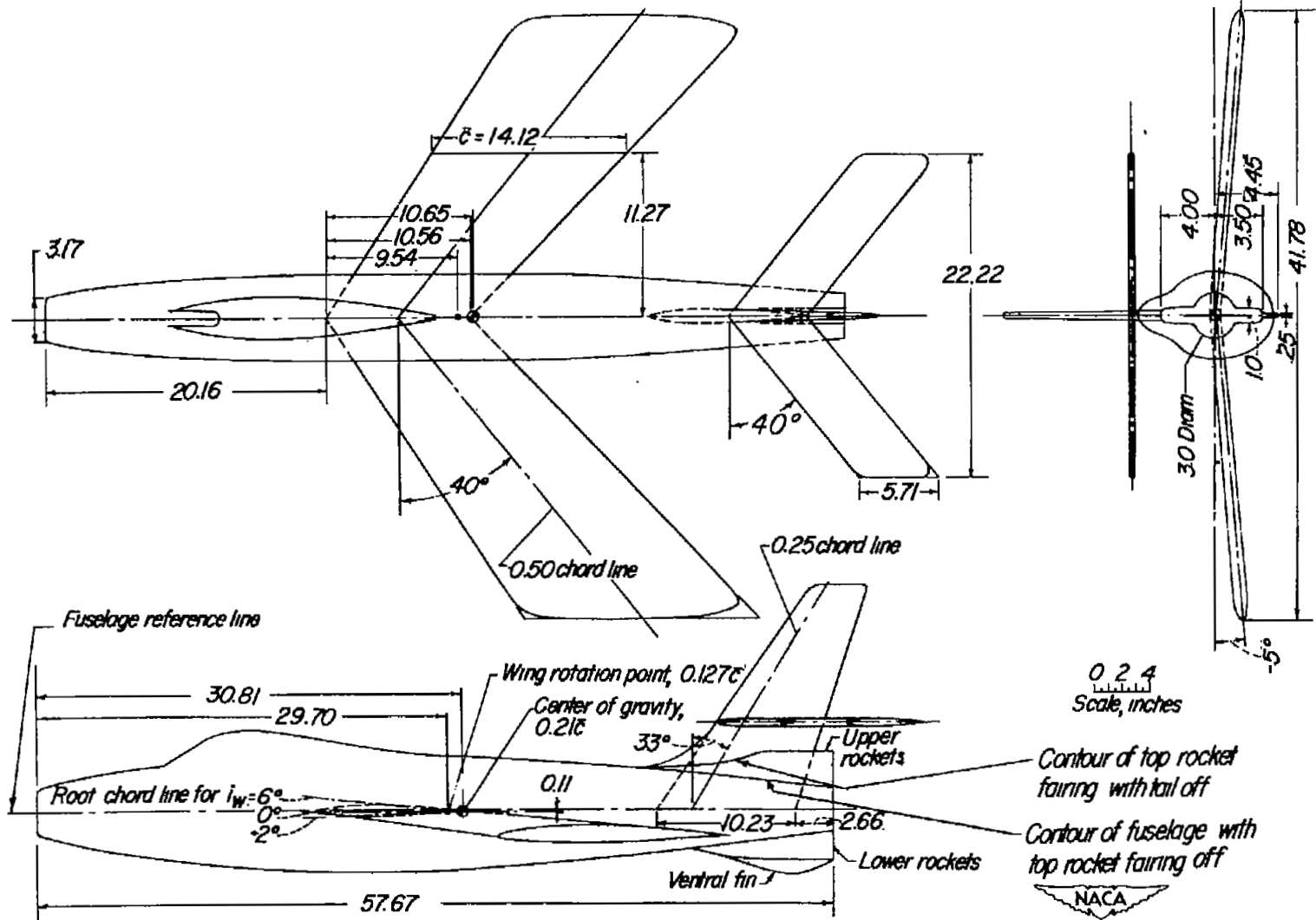
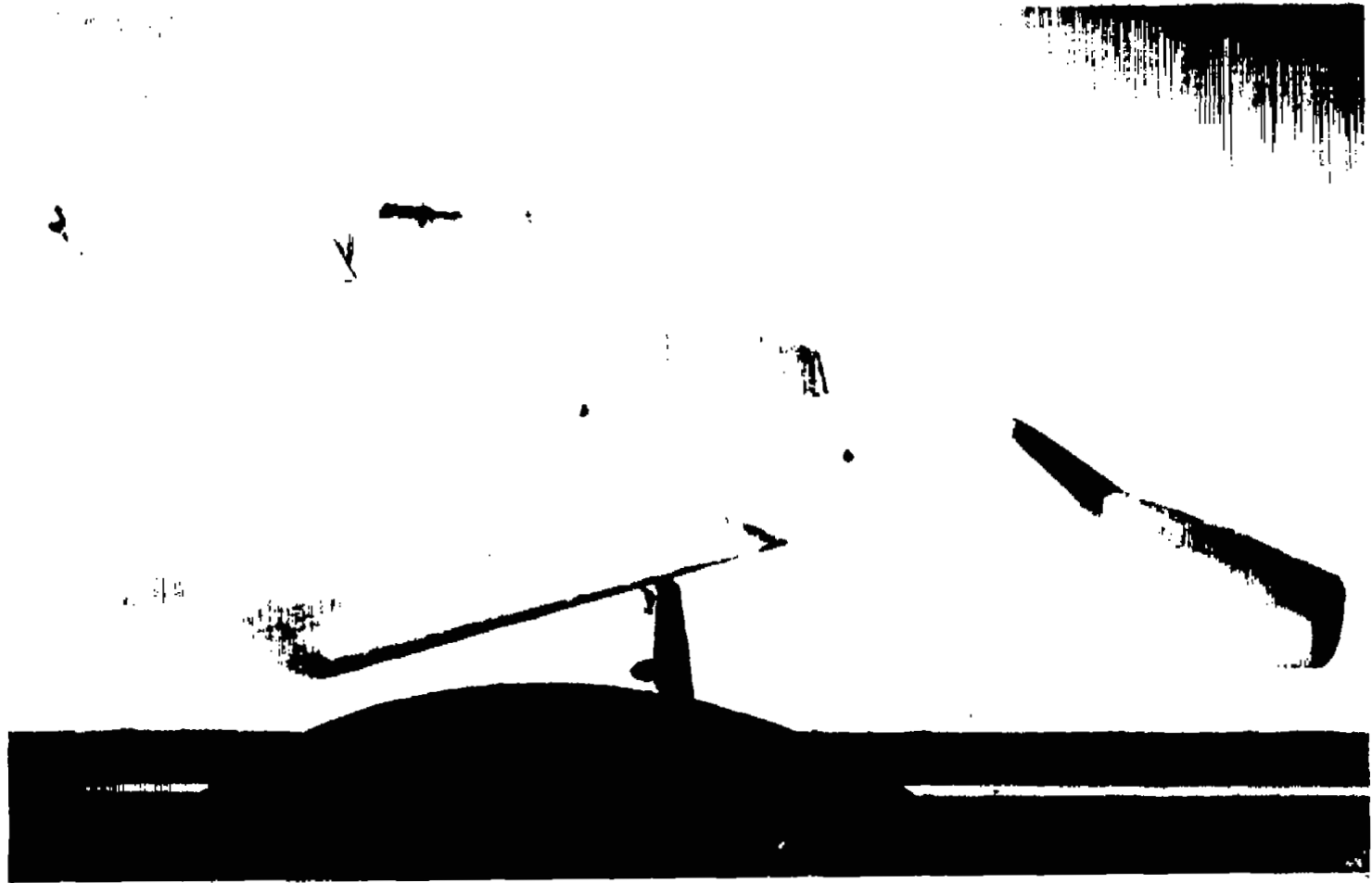


Figure 2.- Geometry of the 1/9-scale model of the Republic F-91 airplane.
All dimensions are in inches.



L-75825

Figure 3.- Three-quarter front view of 1/9-scale model of the Republic F-91 airplane in tunnel.

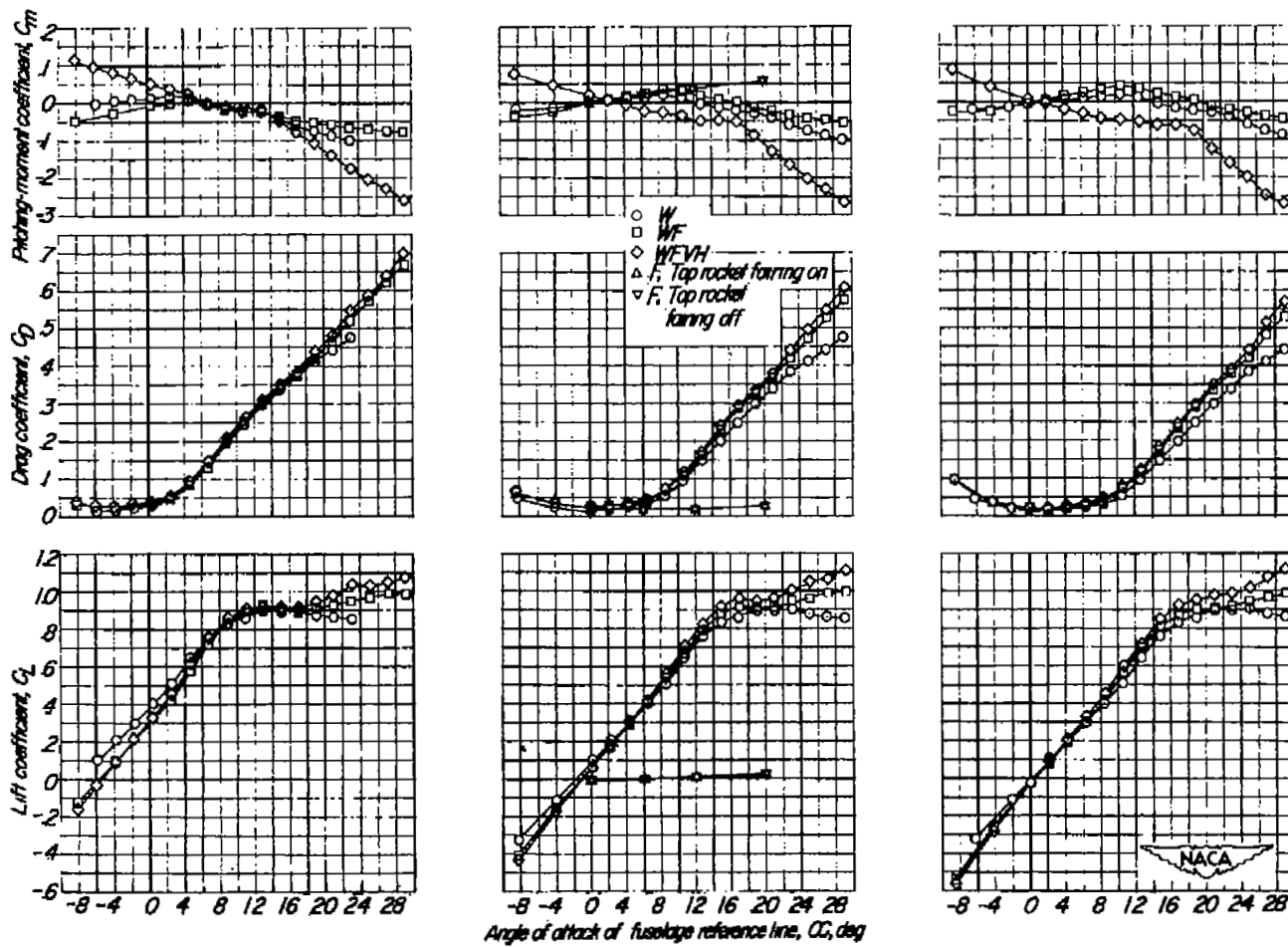


Figure 4.- Variation of C_m , C_D , and C_L with α for a 1/9-scale airplane model of the Republic F-91 airplane. Center of gravity at $0.21\bar{c}$.

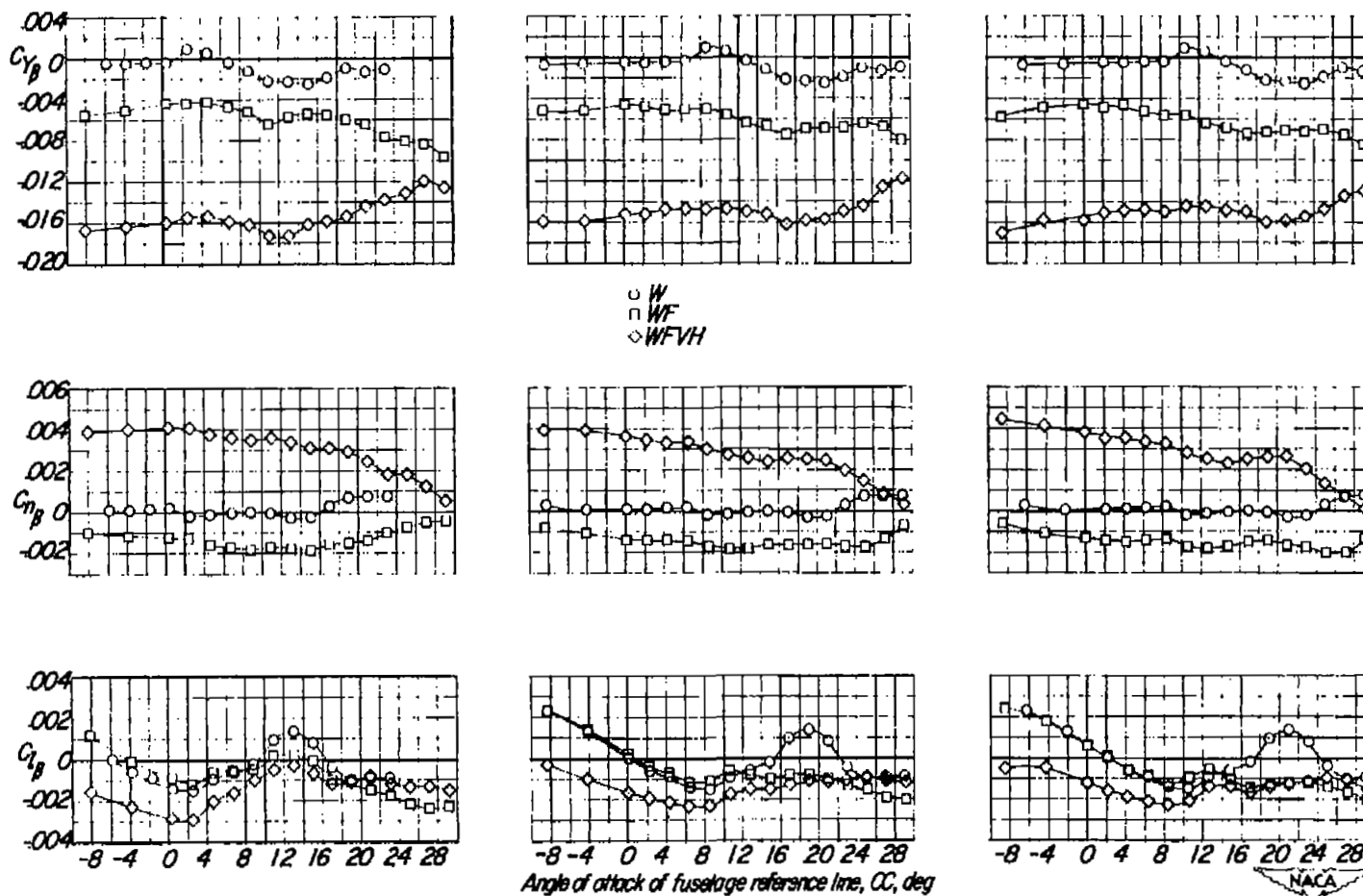
(a) $i_w = 6^\circ$.(b) $i_w = 0^\circ$.(c) $i_w = -2^\circ$.

Figure 5.- Variation of $C_{Y\beta}$, $C_{n\beta}$, and $C_{l\beta}$ with α for a 1/9-scale airplane model of the Republic F-91 airplane. Center of gravity at $0.21\bar{c}$.

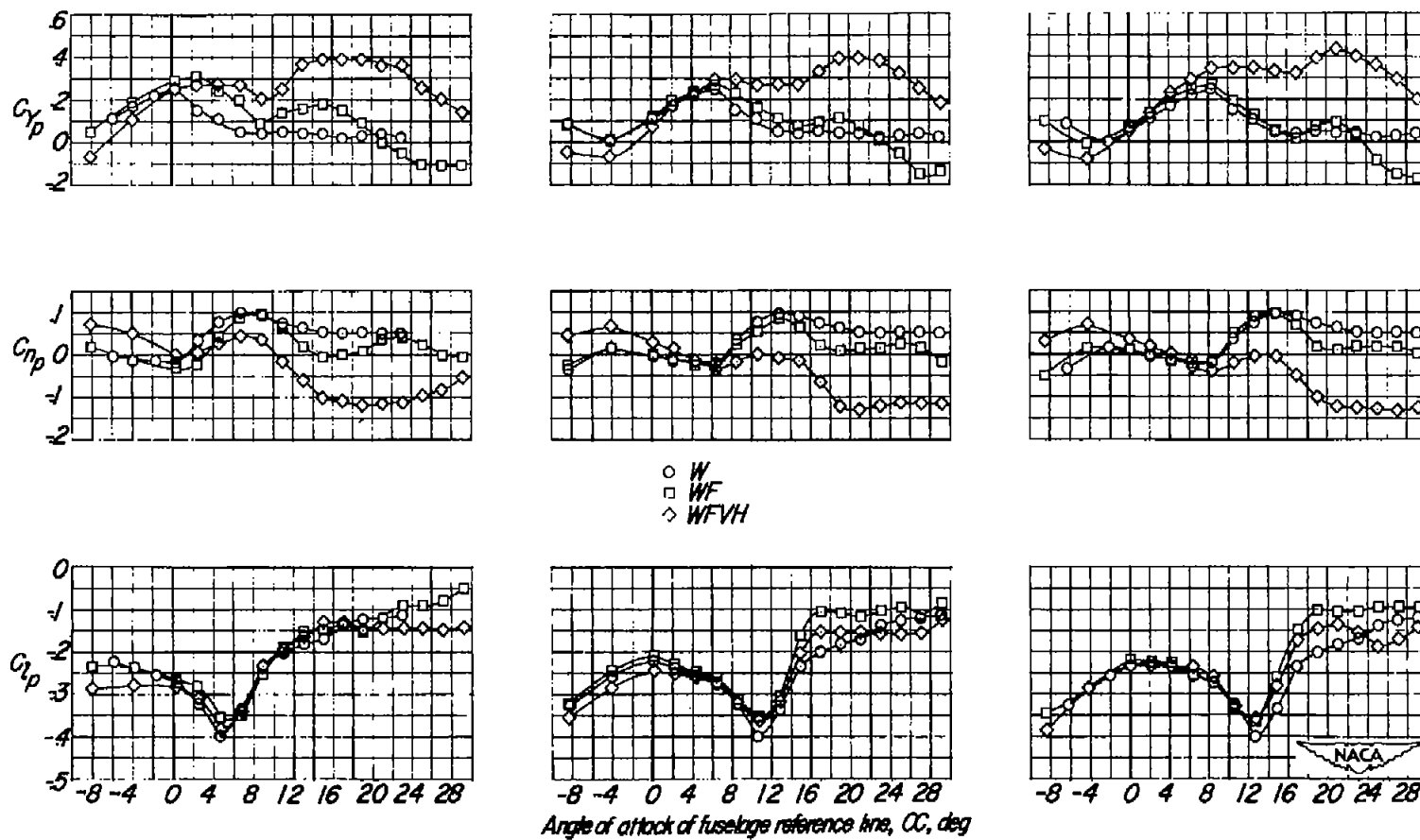
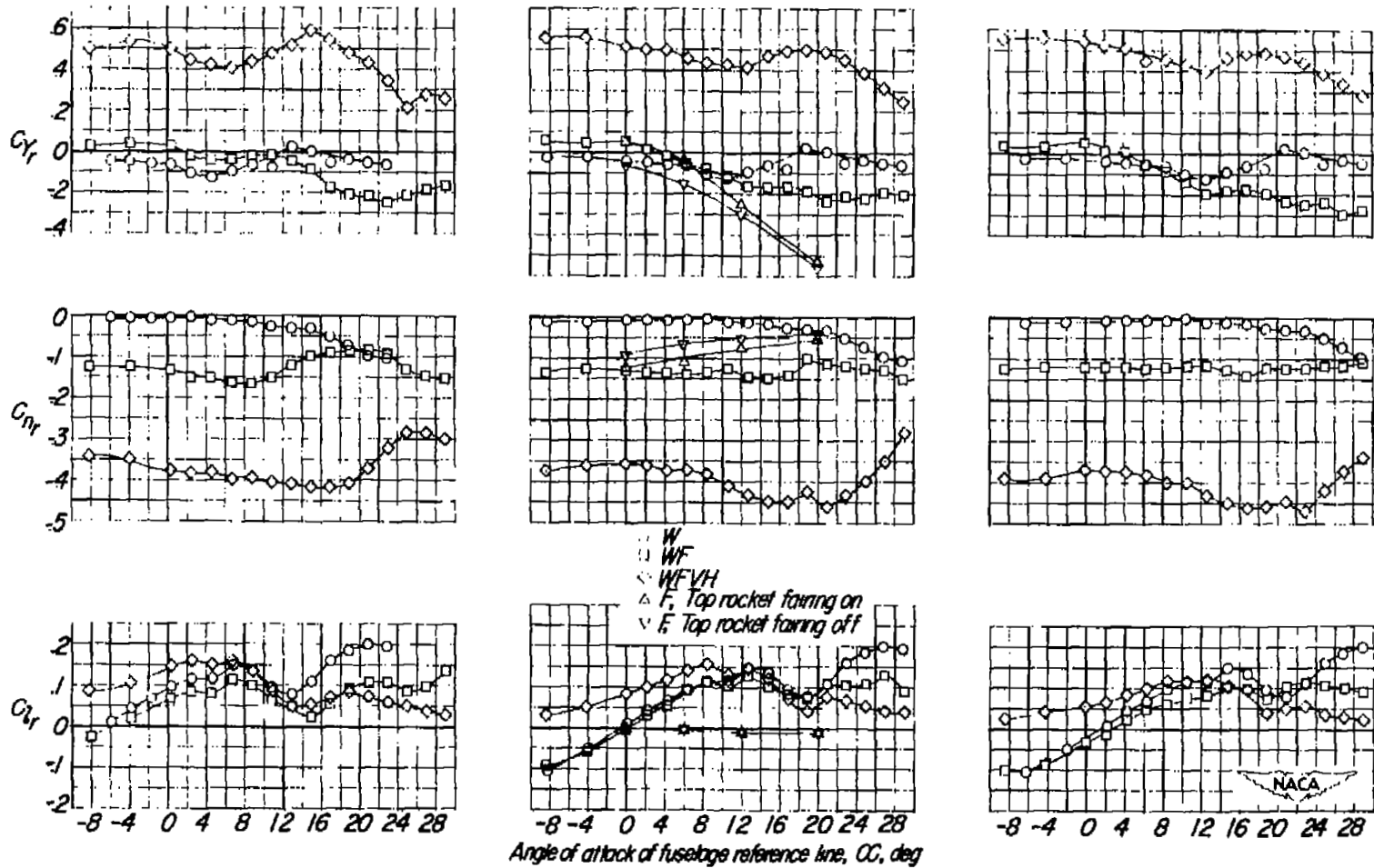
(a) $i_w = 6^\circ$.(b) $i_w = 0^\circ$.(c) $i_w = -2^\circ$.

Figure 6.- Variation of C_{Y_p} , C_{N_p} , and C_{L_p} with α for 1/9-scale airplane model of the Republic F-91 airplane. Center of gravity at $0.21\bar{c}$.

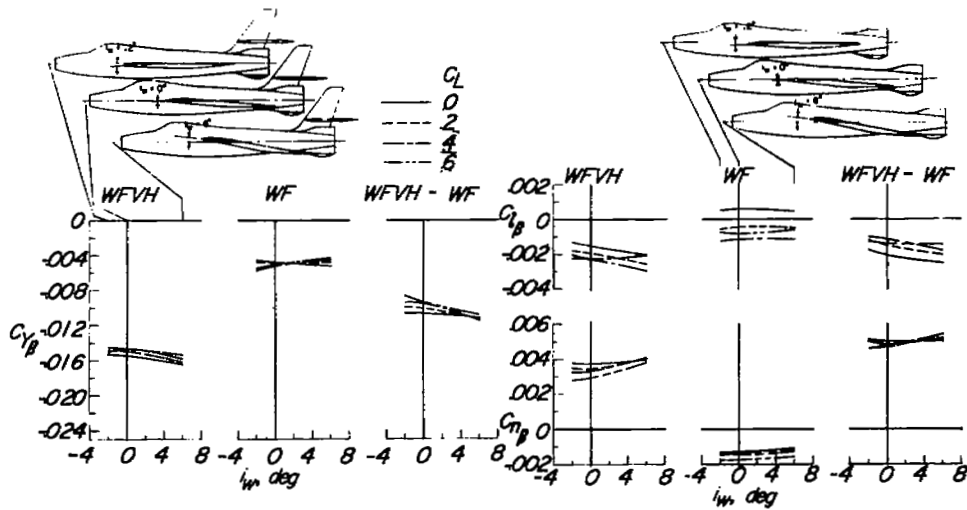


(a) $i_w = 6^\circ$.

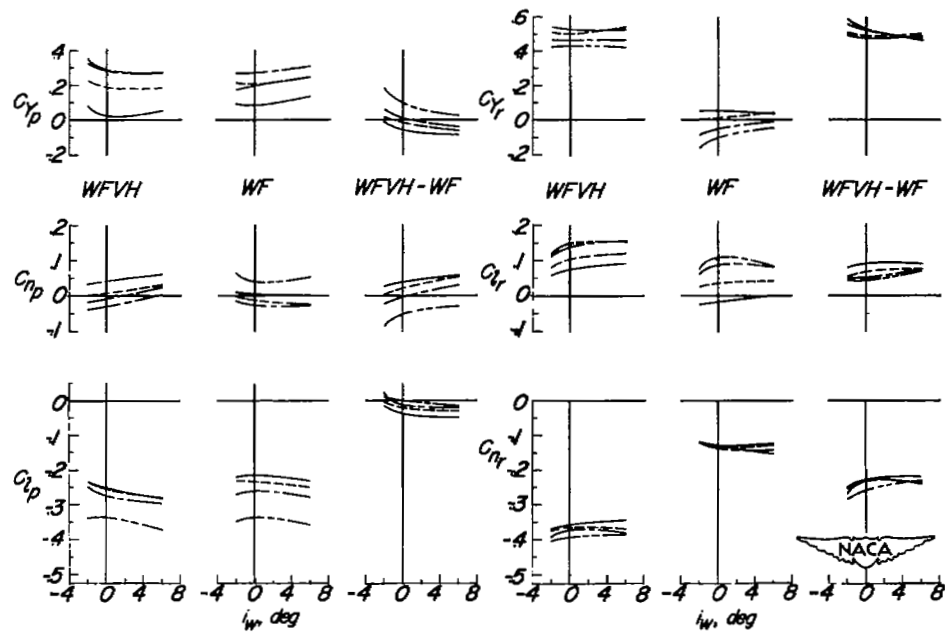
(b) $i_w = 0^\circ$.

(c) $i_w = -2^\circ$.

Figure 7.- Variation of C_{Y_r} , C_{N_r} , and C_{L_r} with α for a 1/9-scale airplane model of the Republic F-91 airplane. Center of gravity at $0.21\bar{c}$.



(a) Variation of static derivatives of WFVH, WF, and WFVH-WF with i_w .



(b) Variation of rolling derivatives of WFVH, WF, and WFVH-WF with i_w .

(c) Variation of yawing derivatives of WFVH, WF, and WFVH-WF with i_w .

Figure 8.- Effect of wing incidence on static, rolling, and yawing derivatives of a 1/9-scale airplane model of the Republic F-91 airplane.

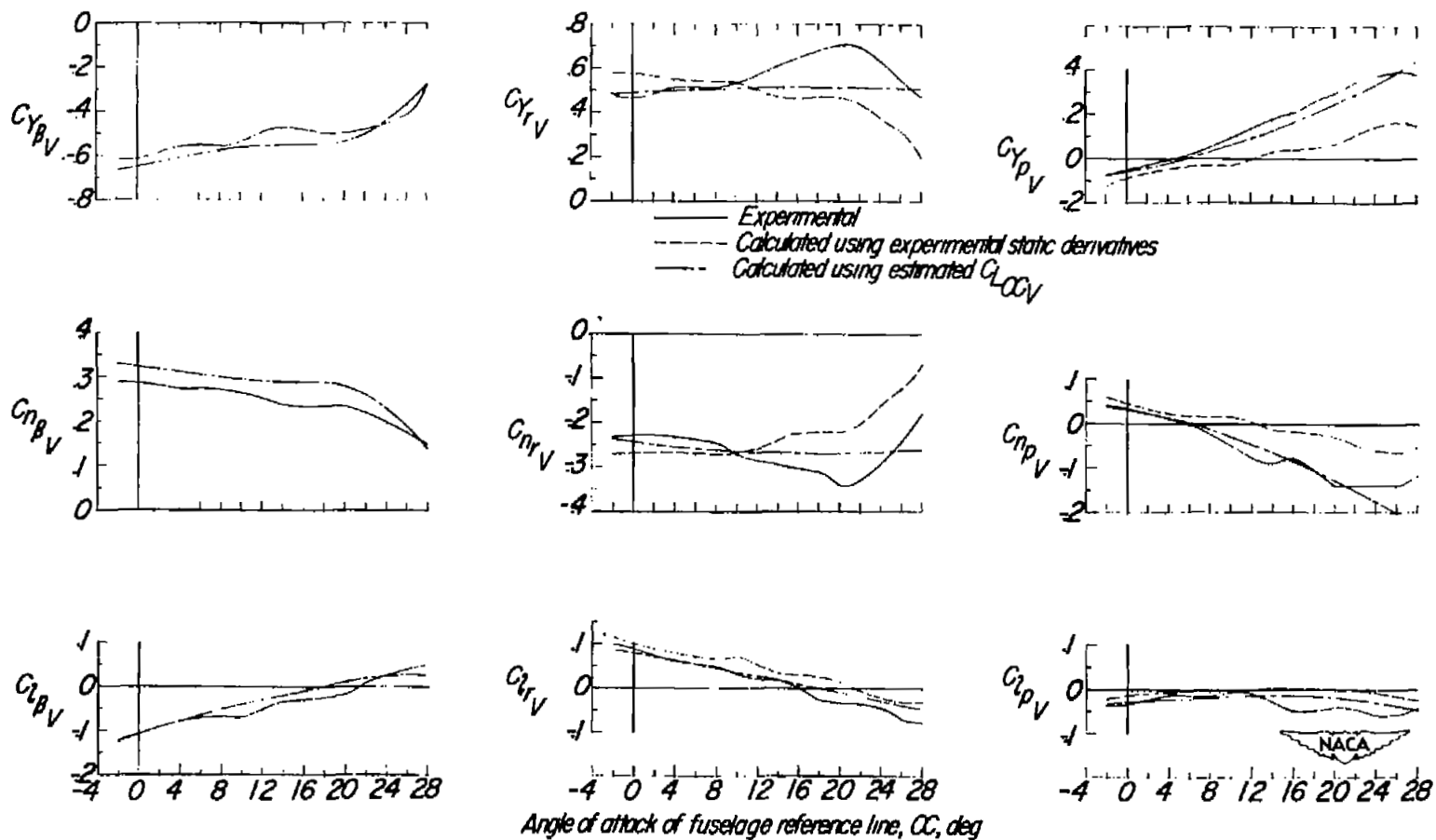


Figure 9.- Comparison of calculated and experimental contribution of vertical tail to static and rotary derivatives. Static derivatives per radian. $i_w = 0^\circ$.

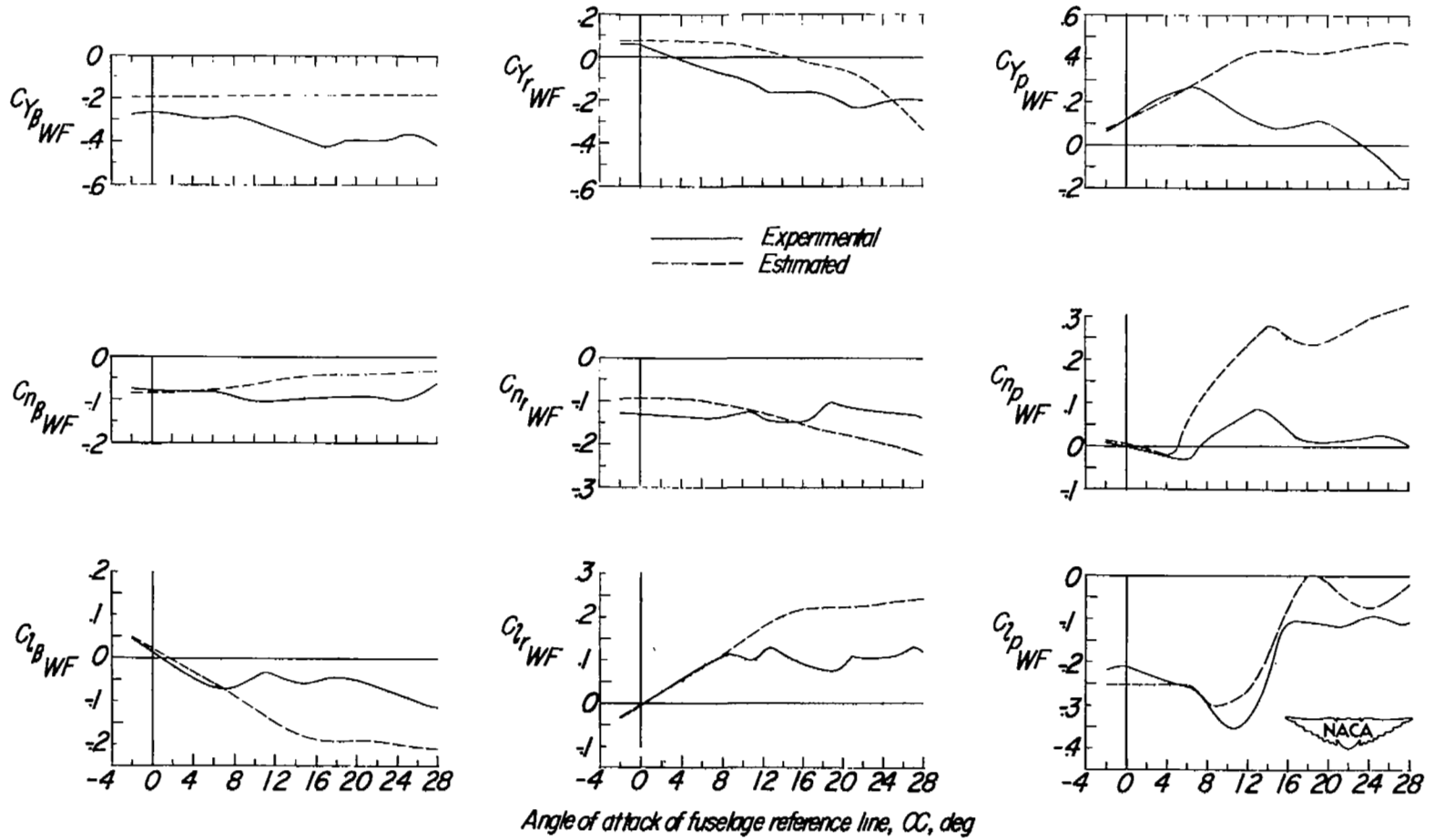


Figure 10.- Comparison of estimated and experimental static and rotary derivatives of wing-fuselage combination. Static derivatives per radian. $i_w = 0^\circ$.

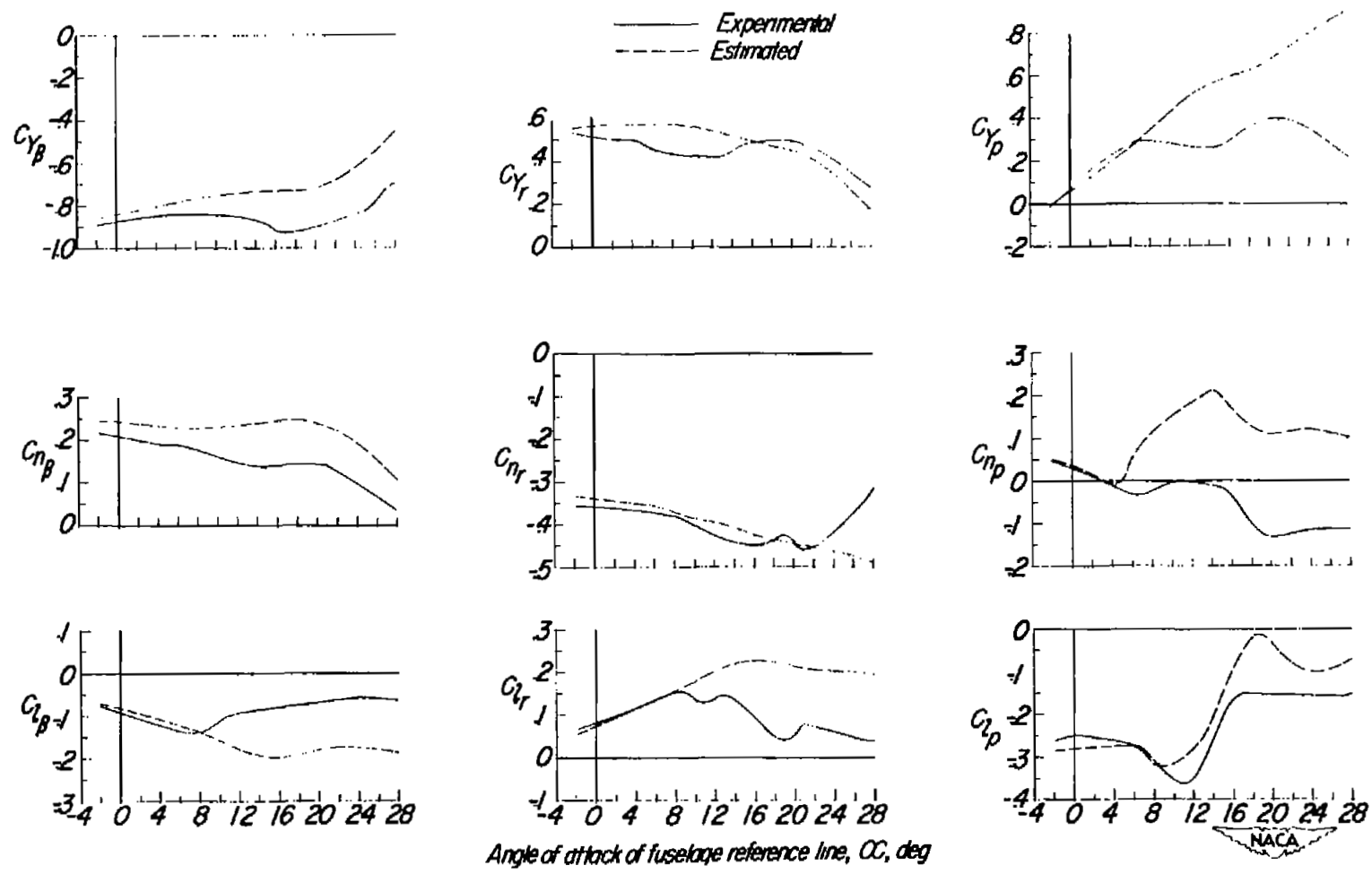
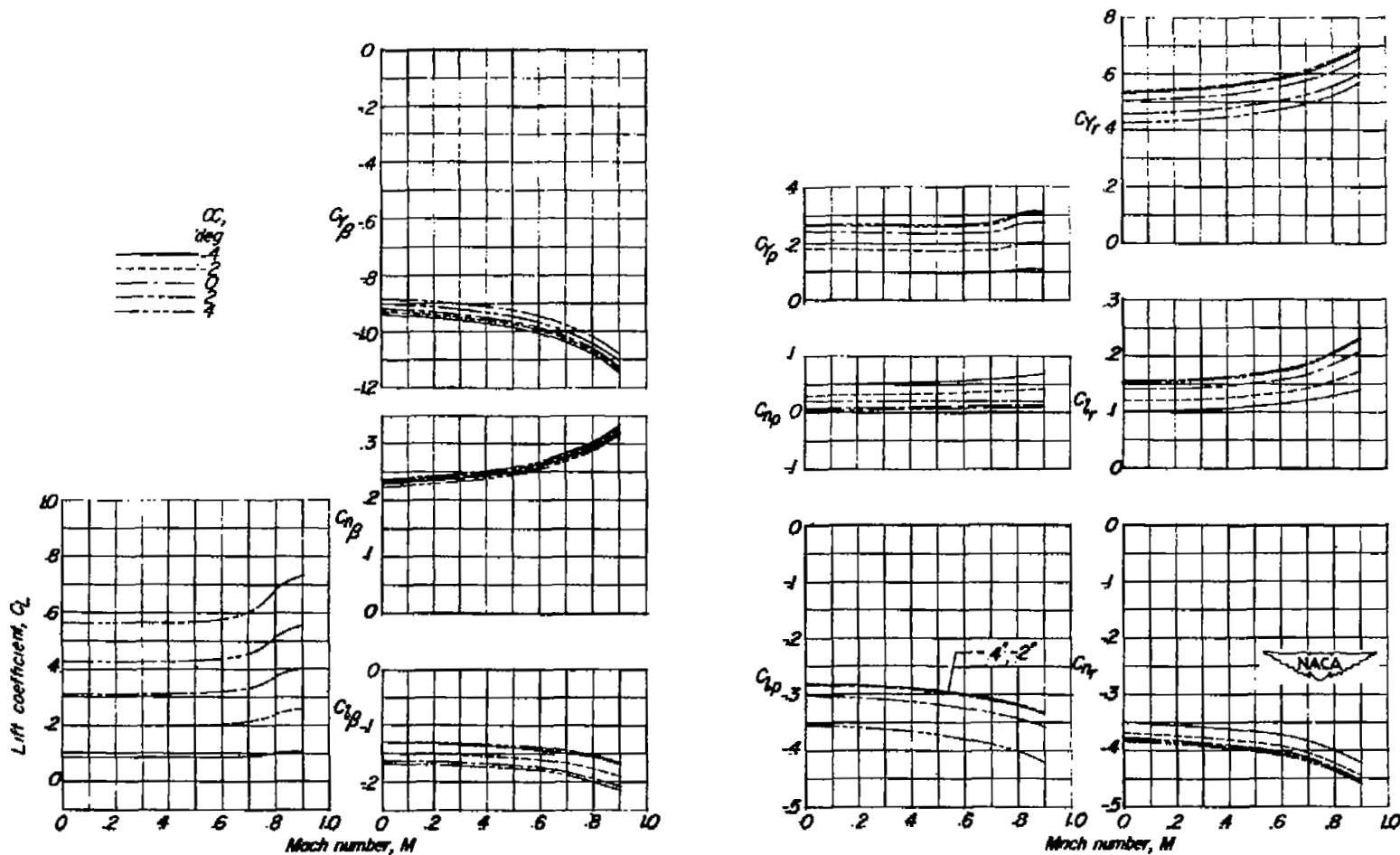
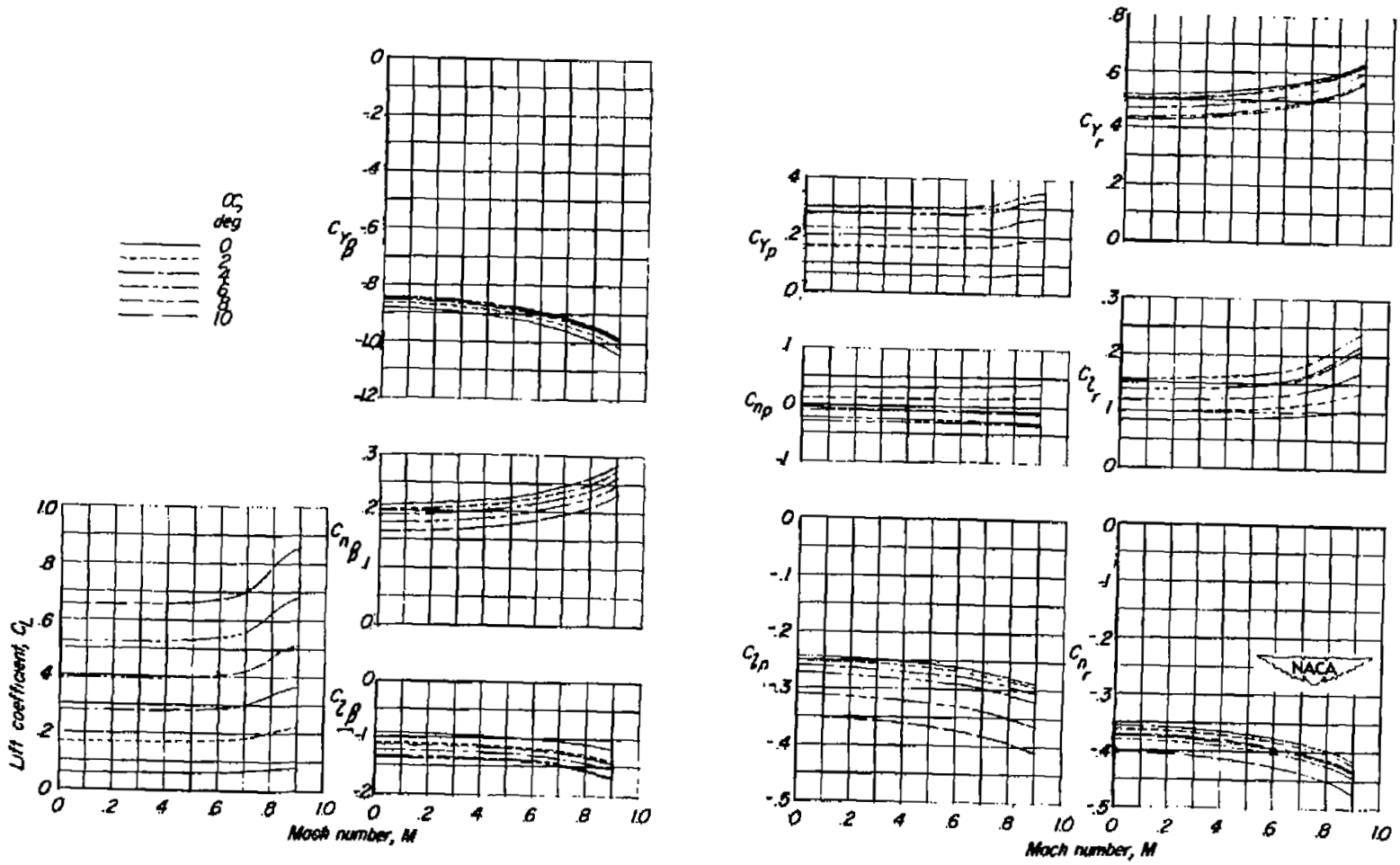


Figure 11.- Comparison of estimated and experimental static and rotary derivatives of complete model. Static derivatives per radian. $i_w = 0^\circ$.



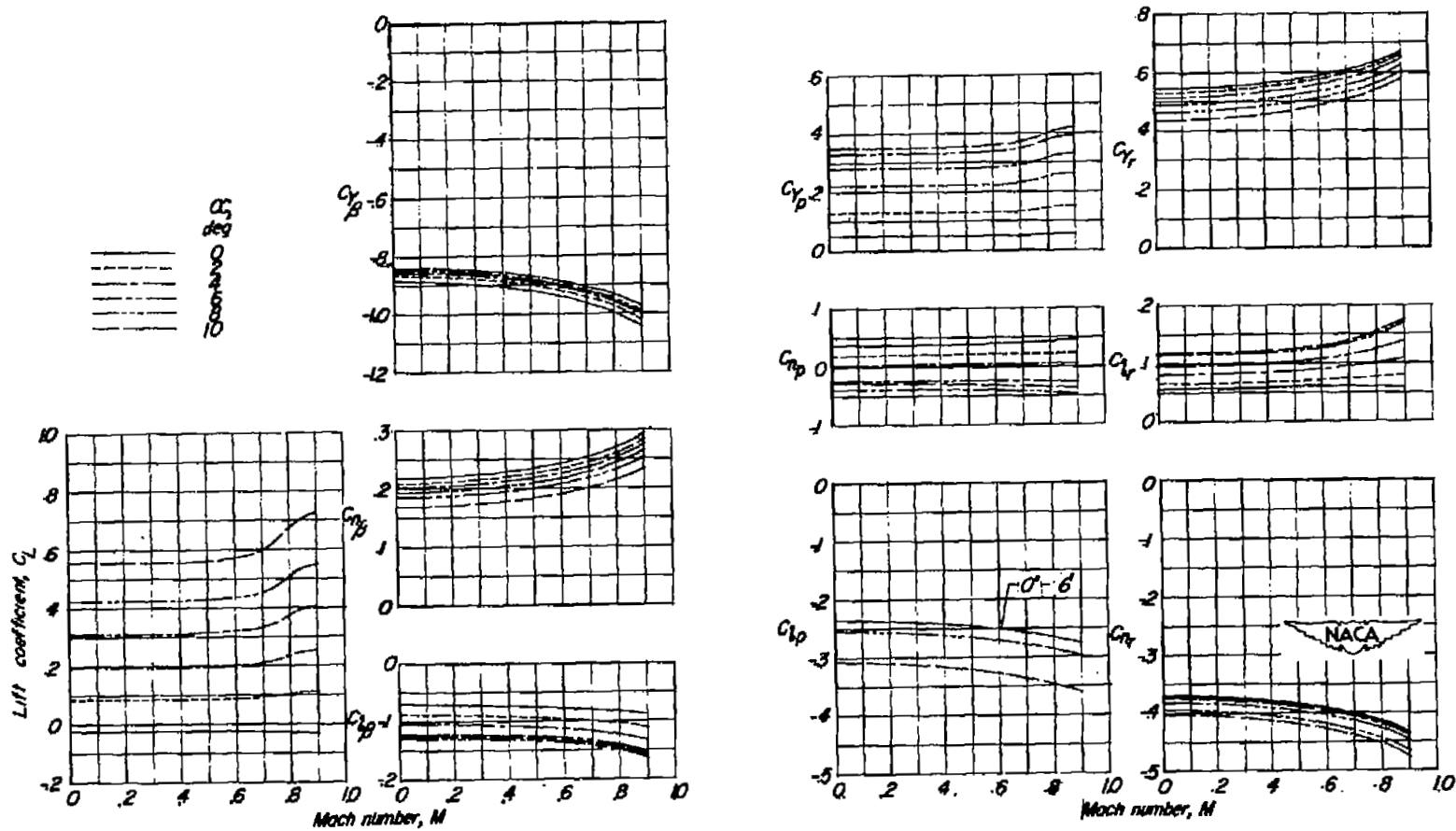
(a) $i_w = 6^\circ$.

Figure 12.- Variation of C_L and static, rolling, and yawing derivatives with Mach number for several angles of attack.



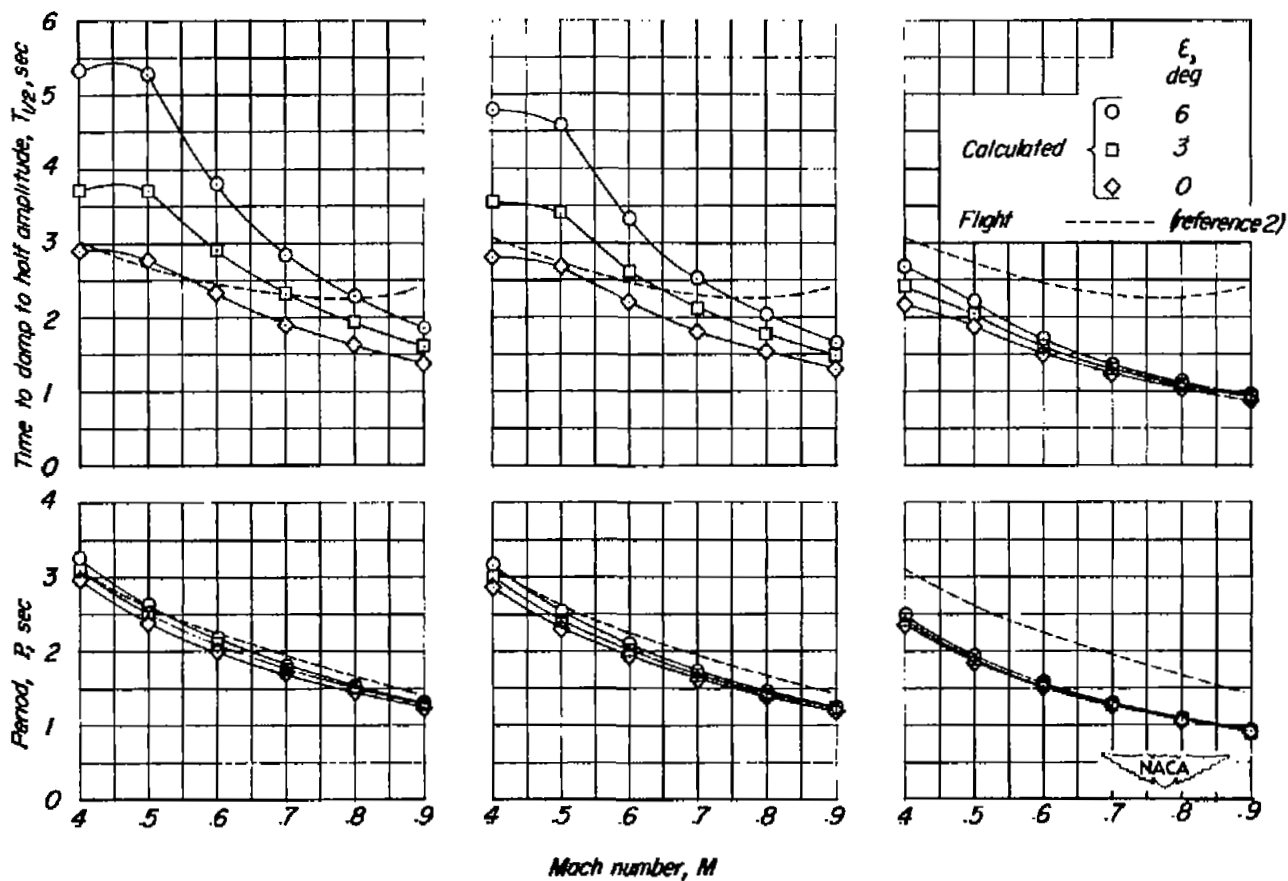
(b) $i_w = 0^\circ$.

Figure 12.- Continued.



(c) $i_w = -2^\circ$.

Figure 12.- Concluded.



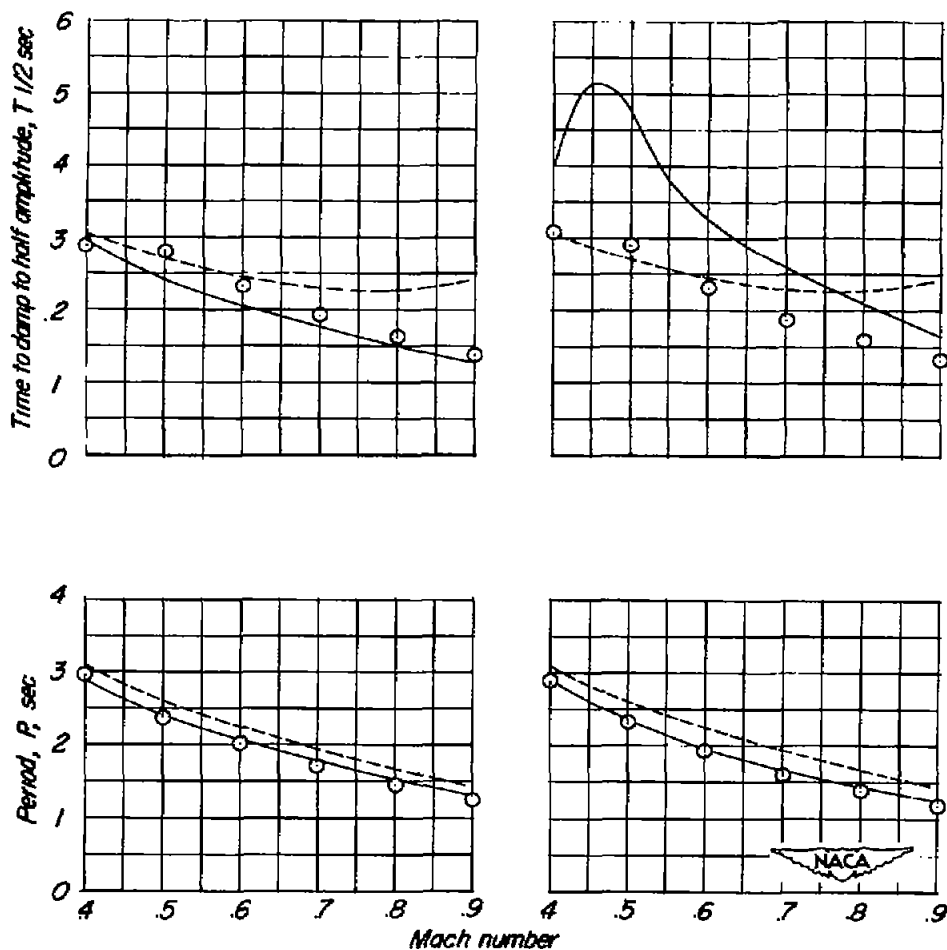
(a) $K_{z_0}^2 = 0.1026$.

(b) $K_{z_0}^2 = 0.0941$.

(c) $K_{z_0}^2 = 0.0544$.

Figure 13.- Effect of ϵ and $K_{z_0}^2$ on variation of $T_{1/2}$ and P with Mach number.
 $i_w = 0^\circ$; Altitude, 20,000 feet; $K_{x_0}^2 = 0.0246$.

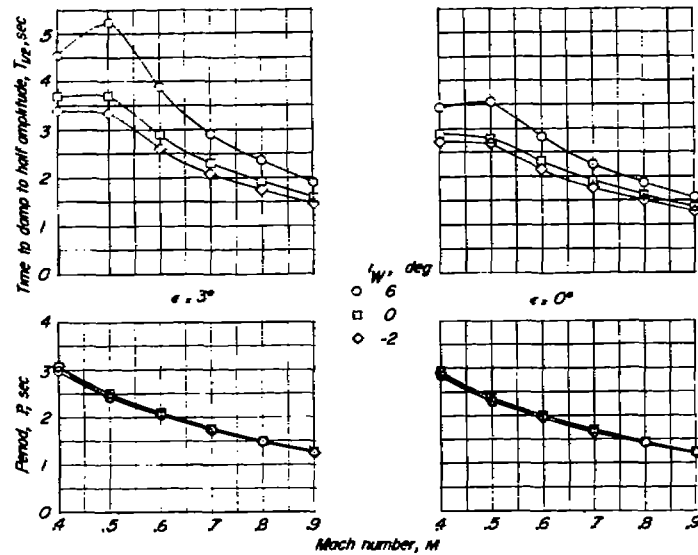
——— Calculated using estimated derivatives, reference 2
 ○ Calculated using experimental derivatives, present paper
 - - - - Flight, reference 2



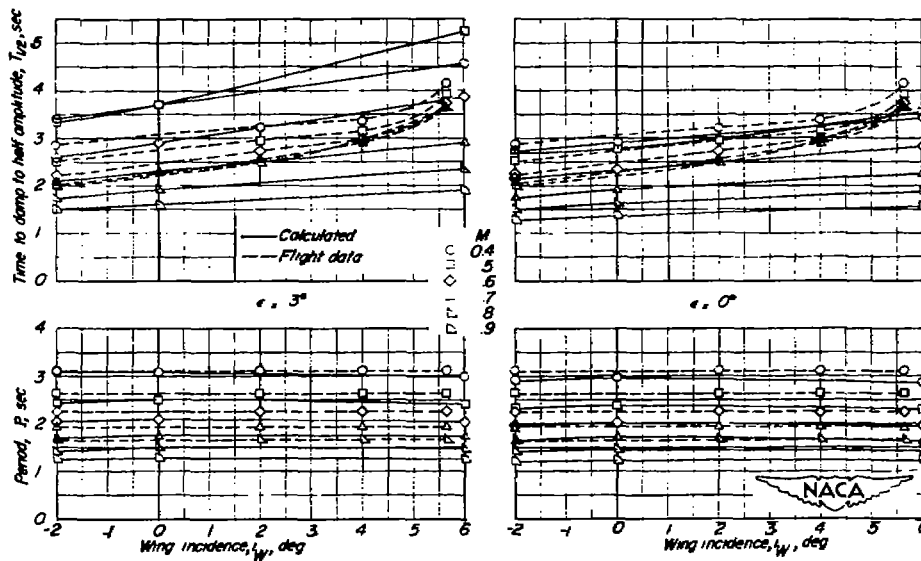
(a) $K_{Z_0}^2 = 0.1026;$
 $K_{X_0}^2 = 0.0246; \epsilon = 0^\circ.$

(b) $K_{Z_0}^2 = 0.0887;$
 $K_{X_0}^2 = 0.0249; \epsilon = 1.5^\circ.$

Figure 14.- Effect of using estimated or experimental derivatives in calculating the variation of $T_{1/2}$ and P with Mach number for the Republic F-91 airplane. Altitude, 20,000 feet. (Estimated derivatives for part (a) were obtained from data related to the investigation of ref. 2.)



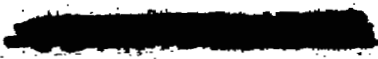
(a) Variation of $T_{1/2}$ and P with Mach number for three wing incidences.



(b) Variation of $T_{1/2}$ and P with wing incidence for several Mach numbers.

Figure 15.- Effect of wing incidence on $T_{1/2}$ and P of lateral oscillation. Altitude, 20,000 feet; $K_{Z_0}^2 = 0.1026$. Flight data obtained from NACA High-Speed Flight Research Station at Edwards Air Force Base, Calif.

SECURITY INFORMATION



LANGLEY RESEARCH CENTER

3 1176 01355 2717

